

Meticulous Object Segmentation

Chenglin Yang^{1*}, Yilin Wang², Jianming Zhang², He Zhang², Zhe Lin², Alan Yuille¹
¹Johns Hopkins University ²Adobe Inc.

{chenglin.yangw, alan.l.yuille}@gmail.com {yilwang, jianmzha, hezhan, zlin}@adobe.com

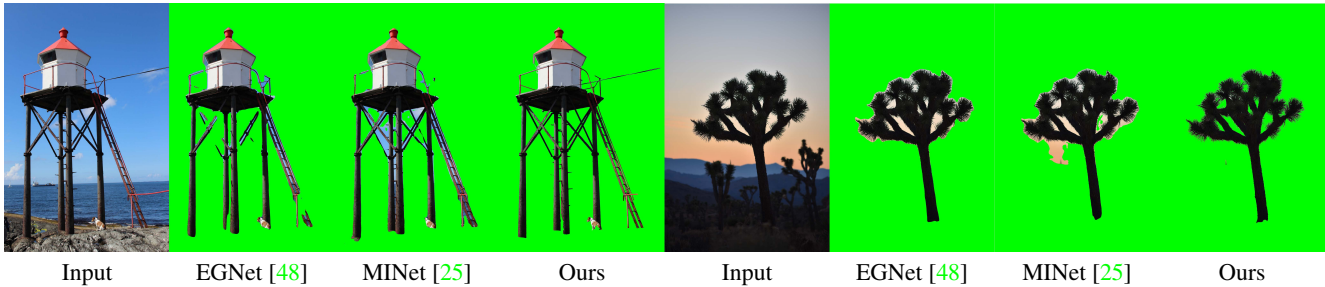


Figure 1: A visual comparison of different methods by compositing the foreground object on green background. See more examples in Figure 8, 9, 10 and 11. Best viewed with zoom-in.

Abstract

Compared with common image segmentation tasks targeted at low-resolution images, higher resolution detailed image segmentation receives much less attention. In this paper, we propose and study a task named Meticulous Object Segmentation (MOS), which is focused on segmenting well-defined foreground objects with elaborate shapes in high-resolution images (e.g. 2k - 4k). To this end, we propose the MeticulousNet which leverages a dedicated decoder to capture the object boundary details. Specifically, we design a Hierarchical Point-wise Refining (HierPR) block to better delineate object boundaries, and reformulate the decoding process as a recursive coarse to fine refinement of the object mask. To evaluate segmentation quality near object boundaries, we propose the Meticulousity Quality (MQ) score considering both the mask coverage and boundary precision. In addition, we collect a MOS benchmark dataset including 600 high quality images with complex objects. We provide comprehensive empirical evidence showing that MeticulousNet can reveal pixel-accurate segmentation boundaries and is superior to state-of-the-art methods for high-resolution object segmentation tasks. The code is publicly available².

*Work done while an intern at Adobe.

²https://github.com/Chenglin-Yang/MOS_Meticulous-Object-Segmentation

1. Introduction

With mobile camera devices and digital imaging tools being used more and more extensively, current applications, such as image editing and manipulation, become more popular and bring forward large demands on techniques of foreground object segmentation [1, 28]. Importantly, these real-world use cases require the techniques to run on high resolution images.

As the resolution of an image going up, more details are revealed by the increasing number of pixels, such as animal furs, human hairs, insect antennas, flower stamens, cavities inside jewelry, handrails at boats, etc. These phenomena around object boundaries increase the difficulty for foreground segmentation at high resolution to pursue good qualities. Unfortunately, most of existing object segmentation works [48, 25] focus on low resolution images, where fine-grained details constituting the object boundaries are not well represented and ignored in the model design. On the other hand, directly processing high resolution image such as 4K resolution will be memory expensive and hard to recover those details [32, 5]. To address these challenges and investigate model capabilities in the computer vision community, we propose and study a task named Meticulous Object Segmentation (MOS).

To distinguish MOS from the traditional task Salient Object Detection (SOD), let's start with some examples shown in Figure 1. The watchtower along the coast is supported by a architecture with cross-linked wooden poles which to-

gether with the ladder and handrails make the object boundaries very complicated. The two state of the art SOD models [48, 25] are able to segment the object body but fail to capture the boundaries. It is the same scenario for the pine tree. The thick branches criss-cross, making the models unable to discriminate the foreground and backgrounds near the branches. These observations indicate that existing SOD methods may not sufficient for MOS. Inherited from visual saliency [10, 2] in computer vision, SOD aims at detecting salient object in an image, while how to precisely capture object details is not fully considered. By contrast, MOS is designated for meticulously segmenting out complex foreground objects. For example, as shown in the Figure 1, our method for MOS successfully deal with these boundary and structure details.

Task Datasets: To ensure fair comparisons and enhance the importance of model developments, we limit the training data to be a collection of current public SOD datasets which is illustrated in Section 4.3. To evaluate MOS methods, we release a testing set MOS600 consisting of 600 high resolution images, whose ground truth masks are carefully annotated. These images contain objects with complicated shapes, and we quantitatively measure their complexity in Section 4.2.

Task Metrics: the evaluation metric for MOS is supposed to consider both the object bodies and boundaries of segmentation masks. Traditional metrics IoU and mBA can evaluate the performance in these two perspectives separately. Besides, we invent Meticulosity Quality (MQ), depicted in Section 4.1, to measure the boundary quality in a moderate way by also considering the mask coverage, as required by MOS. All these metrics are important to measure MOS performance.

To tackle this challenging task, we propose **MeticulousNet**, standing for the network equipped with our designed decoder recovering detailed segmentation boundaries. It includes the following designs: First, it is internally embedded with hierarchical point-wise refining blocks in the decoder layers. This structure enables the network to self-evaluate the uncertainty maps and take them as guidance for the local refinements. Second, we integrate a recursive mask-wise global refinements into the decoder coupled with local modules, boosting the performance by iteratively improving the quality of object masks in higher resolution. As shown in Figure 2, our framework consists of a low resolution segmentation model and a high resolution refinement model. In spite of the different functionalities of these models, they share the same architecture that we designed, MeticulousNet. We use the `_L` and `_H` to discriminate them, indicating low and high quality of the model inputs.

We experimentally study MOS in Section 4.5 and 4.6, where we evaluate MOS methods on HRSOD [39] and MOS600 using both traditional metrics and MQ. Our con-

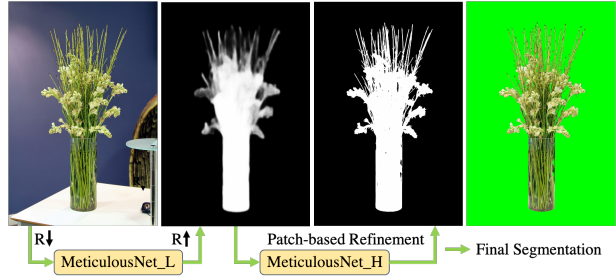


Figure 2: Our framework pipeline. The arrows indicate the resolution (R) change. The input image is first resized to a low resolution. MeticulousNet_L predicts a coarse foreground score map which is then resized back. MeticulousNet_H refines it to a high quality result which is then binarized as the segmentation mask. The final image shows the composite of the segmented foreground and green background.

tributions can be summarized as following:

- (1) We propose Meticulous Object Segmentation (MOS), a foreground segmentation task on high resolution images with complex object boundaries. To evaluate MOS performance, we release MOS600 and invent Meticulosity Quality representing the natural challenges and requirements of integrating body and boundary segmentation in the high resolution scenarios.
- (2) We propose MeticulousNet with a powerful decoder incorporating the hierarchical local refinements and recursive global refinements under the internal unsupervised spatial guidance. This decoder is developed to recover complex foreground boundaries which is used to tackle MOS.

2. Related Work

Meticulous Object Segmentation (MOS) is proposed as a challenging task. Its difficulty lies in the combination of foreground segmentation and detailed boundary segmentation in the scenario of processing objects with complex shapes at high resolution. In this section, we review traditional tasks and models that tackle these problems separately.

2.1. Salient Object Detection

Salient Object Detection (SOD) is to distinguish the most visually salient objects from the backgrounds in images. Early solutions involve the usage of hand-crafted features [10, 12, 36, 41, 38, 51, 6, 44, 42, 1]. The advent of deep convolutional neural networks (CNN) and their feature representations with enormous flexibility [14, 30, 7, 31, 9] takes SOD methods into CNN-based stage [49, 15, 33], which is followed by the works [35, 20, 23, 45, 43, 21, 46] based on FCN and U-Net [22, 27]. Recently, Zhao *et*

al. proposed EGNet designed with a salient edge detection module which is aimed at assisting in object detection [48]. Later in the work of Pang *et al.*, they designed MINet equipped with aggregate-interaction and self-interaction modules to better handle scale variations [25].

In spite of good performances of these state of the art SOD models, they are only suitable for segmenting the foregrounds out of low resolution images. Because at this scale, the boundary details are missing due to the insufficient number of pixels, and are therefore not significant enough to affect the segmentation qualities. In the experimental comparison between a three-branch SOD framework [39] for larger input size with our MOS method (Section 4.6), we found a large performance drop, > 11% in boundary accuracy at HRSOD in which the objects have more than 9 times less boundary complexities than MOS600 (Section 4.2). Both the goal and model developments of SOD focus on object body segmentation, which prevents SOD techniques from being a powerful tool dealing with high resolution images and complex object boundaries.

2.2. Segmentation Refinement

In order to improve the quality of image segmentation results, refinement techniques have been proposed and explored. Traditional methods include the integration of graphical models [13, 3, 50, 18] with deep neural networks. Later on, individual refining modules appeared [26, 40]. One of the design directions is creating generic plug-in modules enabling internal iterative refinements inside the models. RefineNet, proposed by Lin *et al.*, consists of a cascade of RefineNet units [17]. These units connecting with difference levels of features perform multi-path refinements in the upsampling process inside the network. Kirillov *et al.* proposed PointRend module that iteratively selects the most uncertain regions and refines these regions increasing the resolution to a higher value according to point-wise fine and coarse features [11]. Another direction is creating refiners capable of refining masks that predicted by architecture-agnostic models. CascadePSP proposed by Cheng *et al.* adopts a global-local patch-based recursive refining pipeline and achieves the state of the art refiner performance [5].

The majority of the quality improvements brought about by this independent refiner are on the segmentation mask boundaries, especially for high resolution images. Its cascade network structure makes it possible that better performances are achieved by increasing inference times. Specifically, the input of CascadePSP is the concatenation of the raw image and three previously predicted masks that can be either the same or different in a coarse-to-fine fashion depending on the iteration index. However, the dependence of the cascade structure on the existence of previously predictions limits its usage on the refining task. In this work, we break this limitation, and design a decoder (Section 3) that

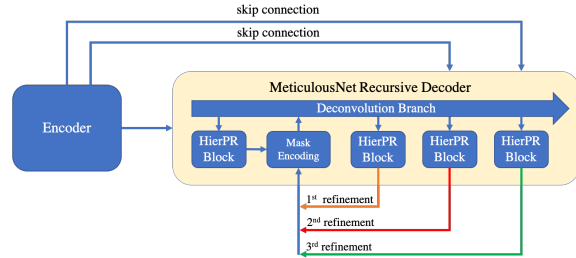


Figure 3: MeticulousNet overview. Orange, red and green arrows represent the recursive processes of the decoder.

can enjoy cascade benefits in both the refining and direct prediction processes.

3. MeticulousNet

Our MOS framework consists two parts with same architecture design: a low resolution MeticulousNet.L segmentation model and a high resolution MeticulousNet.H refinement model. As shown in Figure 2, We first feed the low resolution image to MeticulousNet.L to obtain low resolution mask, then Meticulous.H will crop the high resolution image patch along with low resolution mask to recover mask details in the original resolution. Since both MeticulousNet.L and MeticulousNet.H share the same network design, we describe MeticulousNet in the following.

3.1. Overview

The overview of MeticulousNet is shown in Figure 3. It adopts encoder-decoder structure. The encoder can be the feature extraction modules from other networks, in this paper we use the encoder of PSPNet [47] with ResNet50 [7] and MobileNetV3 [8] backbones. What differentiates MeticulousNet from other models lies in the decoding process. We invent a recurrent decoder achieving local and global self-refinements.

3.2. HierPR Block

Fine object boundaries do not cover large portion of the image area, which drives the need of selecting regions containing these details with correct spatial positions and limited number of pixels in order to perform effective local refinements. Based on [11], we design a Hierarchical Point-wise Refining (HierPR) block. It performs local refinements at selected pixels in the low-level feature maps with pixel inputs from high level feature maps in a hierarchical way.

The Basic PointRend (PR) module [11] is a three-layer perceptron. At each point to perform refinements, the input is the concatenation of the feature vector from pre-specified feature activations and the prediction vector from coarse prediction map at that spatial location. The potential resolution inconsistency is dealt with by interpolation. The coarse

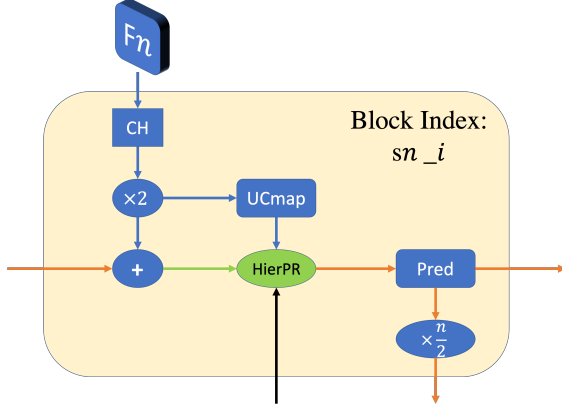


Figure 4: HierPR block. F_n represents the feature maps with output stride n w.r.t. the input size. CH represents the coarse head predicting result, which is formed by two 1×1 convolutional layers. UCmap means the uncertainty map which is used as guidance to perform refinements. HierPR is a three-layer perceptron and Pred is the prediction map after HierPR refinements. HierPR block needs three inputs: pre-specified feature maps from the encoder, feature maps from the deconvolutional layers, predictions from previous HierPR block, which are indicated by the black, blue and orange arrows. i is the cycle index in decoder shown in Figure 5.

prediction is also fed into the intermediate layers for better performance. Since it is computationally infeasible to apply PR at all possible points, an estimated uncertainty map is introduced to provide guidance and limit computation costs. The values in this map are calculated as the absolute distances between the coarse prediction and 0.5 in this binary setting. Then a sorting is performed and a pre-configured number of most uncertain locations are selected to apply refinements. The initial reason why we apply PointRend is to utilize its structure constrain to make the model learn to locate where the object boundaries are in an unsupervised way.

Based on this point-wise processing unit, we propose a hierarchical refinement structure within the basic element HierPR block, which is visualized in Figure 4 and 5. From a macro view, our decoder is an unification of two branches. The first one recovers the resolution of feature maps through deconvolutional layers to the strides of 8, 8, 4 and 2 gradually. The second one refines the coarse outputs coming from the deconvolution branch, or an averaged combination of outputs from both branches (stride 4 and 2), to the strides of 4, 4, 2 and 1 respectively, by means of point-wise refinements. From a micro view, the skip connection pattern differs in these two branches. The last two deconvolutional layers are connected to the first block and first convolutional layer in the encoder, using features from high to low lev-

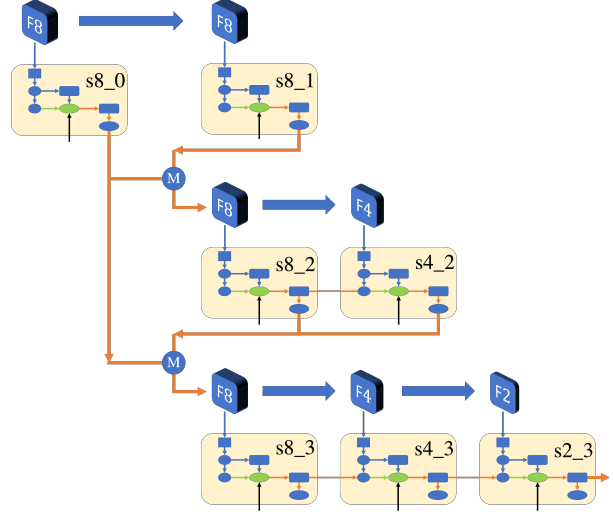


Figure 5: Recursive decoder. The upsampling process proceeds from left to right. The top branch is deconvolution branch and the bottom is refinement branch with HierPR blocks. sn_i represents the block index where n and i represents the output stride of the input feature maps from the top branch to the block and the internal cycle index where this block belongs to. M is the mask encoding layer. The details of each block is shown in Figure 4. The orange arrows show the recursive process. Modules in green share weights globally and those in blue share weights when vertically aligned. See Section 3.3 for details

els. While in the refining branch, all the HierPR modules are only connected to the first block, using the same features to refine all the predictions. These features are relatively low-level when refining the stride 8 prediction but relatively high-level when refining the stride 2 prediction. This contrastive design on the skip connections between two branches enables the HierPR block to provide detail information at low resolution and semantic guidance at high resolution adaptively when doing refinements.

3.3. Recursive Decoder

Complementary to hierarchical local refinements, we design our global refinements in a recursive manner. Inspired by [5] where a complete network is proposed to refine a pre-computed segmentation mask iteratively, we enable our decoder to internally perform global refinements mask-wisely.

As shown in Figure 5, the global refining pipeline in our decoder can be abstracted into two parts. First, it initializes a stride 4 mask by applying an one-time HierPR on a stride 8 coarse features to stabilize the training. Second, there exists a three-cycle upsampling process which is represented in three rows, respectively. These cycles are of different lengths, recovering the resolution to the stride 4, 2 and 1

sequentially via cascade of HierPR blocks. The temporary predicted masks at the end of each internal cycle are concatenated in sequence with the initial stride 4 prediction, which is out of these cycles, as the input to the mask encoding layer. This encodes the coarse-to-fine variations on the predicted masks, which is then utilized to guide global refinements in the next cycle. During training, the supervision are added onto all the intermediate and final predictions, with a weighted combination of binary cross entropy, L1 and L2 losses. (See section 4.4)

Combining both the local and global processes, there are 7 pairs of predictions and 7 uncertainty maps generated by 7 HierPR blocks. We use $S_{n,i}$ to index these blocks where n and i represents the output stride of input feature maps coming from the deconvolution branch and index of internal cycles where this block is. i ranges from 0 to 3 with 0 represents the first prediction outside the 3 latter cycles.

Figure 6 visually records the updates on the uncertainty maps and predictions through these HierPR blocks when the model is fed with an unseen example. The uncertainty maps are grasping the boundaries more and more accurately meaning that our network not only learns a spatial guidance of where to apply refinements correctly but also continuously improves this guidance quality during the upsampling process, which is done in an unsupervised way. Also as shown in the second subfigure, the prediction masks at the end of the recursive cycles provide masks with increasing quality and confidence both locally and globally. All of these behaviors correspond well to our design intention.

4. Experiments

In this section, we propose a metric to quantitatively evaluate Meticulous Object Segmentation (MOS) and release a dataset named MOS600. It contains objects with complex boundaries that are quantitatively measured and serves as the benchmark testing set of MOS. Besides, we also evaluate our methods using traditional metrics and dataset HRSOD [39]. We compare our methods with the corresponding state of the art models in both the low resolution segmentation and high resolution refinement tasks.

4.1. Meticulous Quality

The boundary quality of segmentation masks can be measured by mean Boundary Accuracy (mBA) proposed in [5]. For a given input image with size w and h , N radii are sampled in $[1, \frac{(w+h)}{300}]$ with uniform intervals, which are r_1, \dots, r_N in ascending order. For each r_i , a boundary region b_i is calculated as the difference between the dilation and erosion of the ground truth mask with a circle kernel whose diameter is $2r_i + 1$. Then mBA is calculated as the average pixel accuracy in these N areas. However, to evaluate MOS performance, the segmentation quality of the object body should also be considered. Therefore we invent

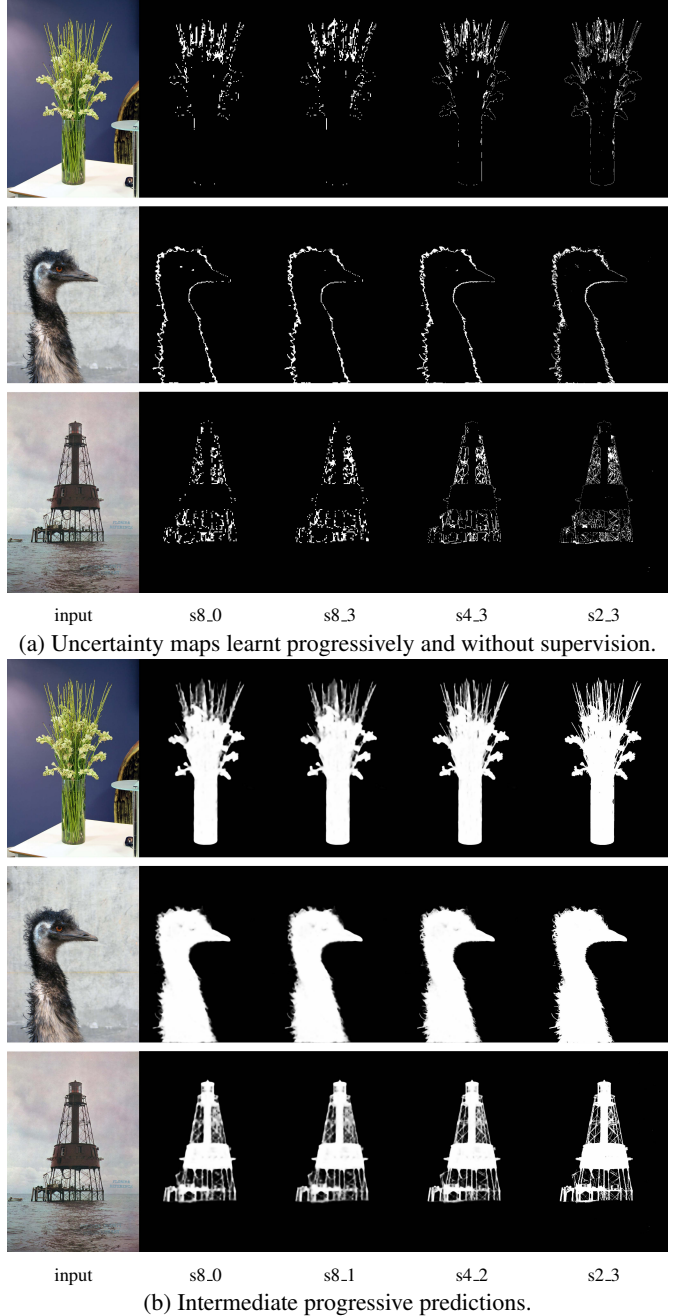


Figure 6: Internal Visualizations of MeticulousNet.H. The first and second subfigures represent the generated uncertainty maps (UCmap) and prediction maps (Pred) in HierPR blocks. The index sn_i corresponds to Figure 5. Best viewed with zoom-in.

Meticulous Quality (MQ), which is calculated as:

$$MQ = \frac{1}{2} P_{b_N}^O + \frac{1}{2N} \sum_{i=1}^N P_{b_i}^I$$

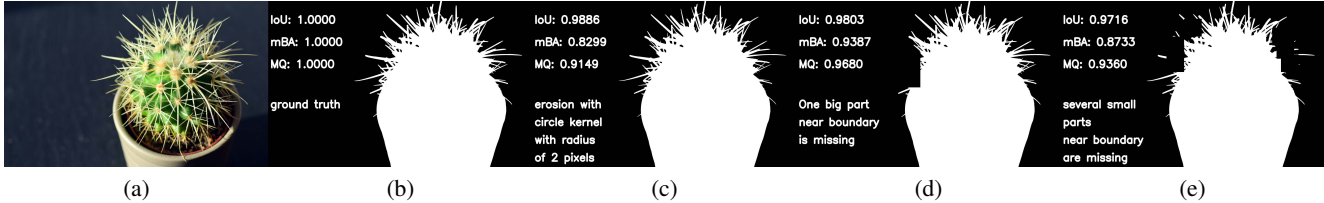


Figure 7: A visual illustration of MQ with IoU, mBA. (a), (b) are the original image and its ground truth mask (GT). (c), (d) and (e) are obtained by perturbing GT. Best viewed with zoom-in.

where $P_{b_i}^I$ and $P_{b_i}^O$ is the pixel accuracy inside and outside the region b_i . The second term comes from mBA, and we set $N = 5$ as well. The reason why mBA is calculated as the average accuracy on 5 different small boundary areas is to ensure the robustness of the measurement for boundaries, which is followed by us. The regions outside b_i can be considered to contain object bodies. Since the area outside is far larger than these small boundary areas, and thus the measurement outside is not affected by several pixel shifts and do not have stability issues. So we just take area outside b_5 to measure body segmentation. MQ of a perfect mask will be 1.

All the metrics IoU, mBA and MQ are important to evaluate Meticulous Object Segmentation (MOS). We provide illustrations in Figure 7. In subfigure (c) where the mask are eroded by 2 pixels, mBA is decreased by a large margin but the visual quality of the segmentation is not affected that severely. In subfigure (d), one big part near object boundary is missing and the visual quality is more harmed than small erosion, but IoU is still as high as that in subfigure (c). Same scenario happens in subfigure (e) where several small parts near boundary are missing, IoU can not well represent missing boundary details while mBA shows large performance degradation although main object body is segmented correctly. MQ provide a perspective to reflect the quality of boundary segmentation in a moderate way. Since IoU and mBA are dedicated in different perspectives, all these metrics are necessary to measure performances of MOS methods.

4.2. Meticulous Benchmark Testing Dataset

We release a dataset of 600 high resolution images with complex boundaries, MOS600. To measure the boundary complexity, we exploit C_{IPQ} [24] as used in [39]. Before the calculation, we crop the patch including the foreground and resize it to be a square as a calibration process. We compare it with the testing set of HRSOD, consisting of 400 carefully annotated high resolution images. As shown in Table 1, the object boundaries in MOS600 are more than 9 times more complex, which shows that MOS600 is a suitable benchmark test set for MOS.

Dataset	$C_{IPQ} (\times 10^{-3}) \downarrow$
HRSOD	11.34
MOS600	1.24

Table 1: Boundary complexity. Lower C_{IPQ} indicates higher complexity. MOS600 is more than 9 times more complex than HRSOD.

4.3. Training Datasets

We train our model using existing datasets. For the low resolution model MeticulousNet_L, we use the training set of DUTS [34] containing 10553 images which have complicated scenes with objects in various scales and locations. For the high resolution model MeticulousNet_H, we exploit the combination of MSRA-10K [6], DUT-OMRON [38], ECSSD [29], and FSS-1000 [16] with 36572 images in total, which is used by [5]. All of these collections contribute to a class-agnostic dataset with objects of diverse semantic categories and various annotation qualities. To enhance the supervision on object details, we add the binarized DIM [37] to the collections. We merge the training and testing sets of DIM and remove the smoke categories, resulting in 463 unique foregrounds. During training when a DIM foreground is sampled, we first compose it with a background image randomly selected from MS COCO [19] and then randomly binarize its alpha map using a threshold randomly generated in the range of 0.1 - 0.5 to get the ground truth segmentation mask. For each training epoch, there are 46300 such compositions.

4.4. Implementation Details

At low resolution, MeticulousNet only uses Binary Cross Entropy loss (BCE) applied on the intermediate and final outputs. The learning rate is adjusted using a cosine annealing schedule, starts from 2.5×10^{-3} and decreases to 0 in 60000 iterations. The input image is resized to 336, and batch size is 20. Data augmentations involve random horizontal flips, rotations, and color jittering as used in [25]. At high resolution, we adopt patch-based training used in [5]. A combination of BCE, L1 and L2 losses are utilized with a triple weights (w_b, w_1, w_2). Corresponding to the

7 HierPR blocks in Table 5, we use (1.00, 1.00, 1.00) for S8_0, S8_1, S8_2, S8_3; (0.50, 0.25, 0.25) for S4_2, S4_3; (0.00, 1.00, 1.00) for S2_3. Gradient loss on the final prediction with a weight of 5 is also added. The learning rate starting with 2.25×10^{-4} is step-wisely decayed by a factor 10 after iterations 22500 and 37500 in a total of 60000. We use a batch size of 24. The inputs are concatenations of 224×224 patches cropped from the original images and their corresponding ground truth masks that are randomly perturbed to have an IoU in the range 0.8 - 1.0 with the unperturbed ones. At both resolutions, we set HierPR to refine 10% pixels in the feature maps. Before training at high resolution, the weights are initialized from the best training epoch on HRSOD at low resolution.

4.5. MeticulousNet at Low Resolution

The goal of MOS is to segment objects from high resolution images, and the design of MeticulousNet aims at capturing complex boundaries. However, since our framework outputs a coarse mask and then refines it, we perform experiments to investigate how well MeticulousNet performs at low resolution. In this case, the resolution challenge disappears and boundary details are not significant for the foreground segmentation. We name our model Meticulous_L and compare it with two state of art models for Salient Object Detection (SOD), EGNet [48] and MINet [25]. We use the model checkpoints released by the authors for fair comparison. For testing sets, we resize HRSOD and MOS600 to the size 336×336 . The predictions on these images by the models are used as the initial masks in the refinement stage which is studied in Section 4.6. Since all comparing methods use DUTS-TR as training set, we also report the comparisons on DUTS-TE.

The experimental results are reported in Table 2, 3 and 4. On DUTS-TE, Meticulous_L achieves the highest MQ, IoU and comparable mBA with EGNet. MINet has a slightly lower value in MAE but gets worst score otherwise. On HRSOD, Meticulous_L shows a small degrade 0.09% in mBA compared with EGNet, but gives the best performance on all other metrics. EGNet is able to handle foreground boundaries properly, and this can attribute to the fact that EGNet has a module predicting object boundary edges and thus receive extra supervision from object edges in the training process. However, when the object boundary complexities increase, its advantage disappear. On MOS600, MeticulousNet_L provides the best performance on all the metrics. MINet does not perform well in mBA on all datasets with an average of more than 1.3% performance gap with others. Together with the performances on DUTS-TE and HRSOD, MeticulousNet_L consistently provides the best performance on object body and boundary segmentation, which is reflected by the highest MQ, highest IoU, and competitive mBA. These properties at low resolution hint

the large potential of MeticulousNet to process high quality data.

Method	MAE ↓	S-m ↑	IoU ↑	mBA ↑	MQ ↑
EGNet	3.91	88.70	78.22	66.44	81.79
MINet	3.69	88.45	78.14	64.76	80.98
MeticulousNet_L	3.76	88.60	78.40	66.42	81.84

Table 2: Low resolution foreground segmentation on DUTS-TE. (Units: 1×10^{-2})

Method	MAE ↓	S-m ↑	IoU ↑	mBA ↑	MQ ↑
EGNet	4.05	89.47	80.19	66.18	81.51
MINet	3.58	89.59	80.49	64.82	80.96
MeticulousNet_L	3.46	89.75	80.59	66.09	81.74

Table 3: Low resolution foreground segmentation on HRSOD. (Units: 1×10^{-2})

Method	MAE ↓	S-m ↑	IoU ↑	mBA ↑	MQ ↑
EGNet	6.89	82.21	70.50	60.54	77.83
MINet	6.55	81.94	69.94	59.30	77.27
MeticulousNet_L	6.40	83.38	72.18	60.72	78.16

Table 4: Low resolution foreground segmentation on MOS600. (Units: 1×10^{-2})

4.6. MeticulousNet for MOS

In this section, we show the experimental results on MOS. Based on predictions from Meticulous_L, which is described in Section 4.5, our framework consists of another MeticulousNet with the same architecture as high resolution refiner, Meticulous_H. To ensure fair comparisons, we set our strong baselines as combinations of the state of the art (SOTA) SOD model and SOTA refiner. We use EGNet and MINet to predict coarse masks, and cascadePSP [5] for refinements. We use the best released checkpoints. Since MeticulousNet_H includes binarized DIM in the training set as mentioned in Section 4.3, we also re-train a model, cascadePSP*, using the same training data. All the other training and testing procedures are ensured the same. We perform comparisons on HRSOD testing set and MOS600 the images of which are never seen by the models. Another baseline methods are GLF networks proposed with HRSOD, and we use their released predicted masks for comparisons.

The experimental results are shown in Table 5. On HRSOD, GLF networks show a large performance gap with our proposed strong baselines. Comparing the baseline methods with cascadePSP and cascadePSP*, we do not observe clear benefits brought by the addition of binarized

Dataset	HRSOD					MOS600					
	Method	MAE ↓	S-m ↑	IoU ↑	mBA ↑	MQ ↑	MAE ↓	S-m ↑	IoU ↑	mBA ↑	MQ ↑
EGNet		4.06	89.39	80.10	64.76	80.91	7.04	81.87	69.99	61.25	78.76
MINet		3.61	89.57	80.41	63.85	80.59	6.70	81.69	69.59	60.13	78.33
GSN+APS+LRN+GLFN		2.98	89.67	80.40	62.26	80.11	---	---	---	---	---
EGNet + cascadePSP		3.56	89.34	81.70	72.32	84.66	5.88	82.59	73.12	67.67	82.04
MINet + cascadePSP		2.98	89.67	82.64	72.32	84.82	5.70	83.00	73.47	67.25	81.99
EGNet + cascadePSP*		3.51	89.29	81.66	72.41	84.72	5.56	83.58	74.69	70.27	83.40
MINet + cascadePSP*		3.23	89.98	82.76	72.56	84.94	5.34	84.13	75.19	69.96	83.40
MeticulousNet_(L+H)		2.97	90.00	82.56	73.64	85.59	5.08	85.08	76.43	72.09	84.46

Table 5: Meticulous object segmentation in high resolution, Note that boundary complexity in MOS is more than 9 times higher than HRSOD. (Units: 1×10^{-2})

DIM data. For example, based on the predictions by MINet, cascadePSP* increases both IoU and mBA by 0.12% and 0.24%, respectively, compared with raw cascadePSP. However, on top of predictions by EGNet, cascadePSP* increases mBA by 0.08% but decreases IoU by 0.04%. Comparing MeticulousNet with all the other baselines, it shows a small degrade in IoU, 0.20% lower compared with cascadePSP* on top of MINet, but has a more than 1% increase in mBA compared with all the baselines. It also achieves the highest performance on all the other metrics.

On MOS600, since the object boundary complexities are increased by more than 9 times than HRSOD as shown in Section 4.2, the differences among different methods are enlarged. MeticulousNet provides the best performance on all the metrics among all the methods. Comparing it with the off-the-shelf cascadePSP on top of SOD models, it increase IoU, mBA and MQ by at least 2.96%, 4.42% and 2.42%, respectively. Comparing the baseline methods, we observe a benefit from the addition of the binarized DIM data. On top of both EGNet and MINet, cascadePSP* improves the performance in MQ by around 1.4% compared with cascadePSP. Comparing this strongest baseline with MeticulousNet, there are consistent improvements on all the metrics. It improves IoU, mBA and MQ by 1.24%, 2.13% and 1.06%. All these experiments verify the superior capability of MeticulousNet to deal with the segmentation of both foreground body and boundary, as required by MOS. See the visual comparisons in Figure 8, 9, 10 and 11.

To better demonstrate the effectiveness of MeticulousNet_H, we compare it with cascadePSP directly in the refinement task on high resolution dataset BIG [5] studied in their paper. We download the segmentation masks pre-computed by the authors using semantic segmentation model DeepLabV3+ [4]. They are used as inputs for all the refinement models. The results are shown in Table 6. Comparing cascadePSP and MeticulousNet, it is observed they show comparable performance in IoU but MeticulousNet shows better performance in boundary segmentation by an increase of 0.18% in mBA, which is also reflected in

Method	IoU ↑	mBA ↑	MQ ↑
cascadePSP	92.22	74.67	86.74
MeticulousNet	92.23	74.85	86.84
cascadePSP*	92.02	74.34	86.56
MeticulousNet_H	91.96	75.32	87.03

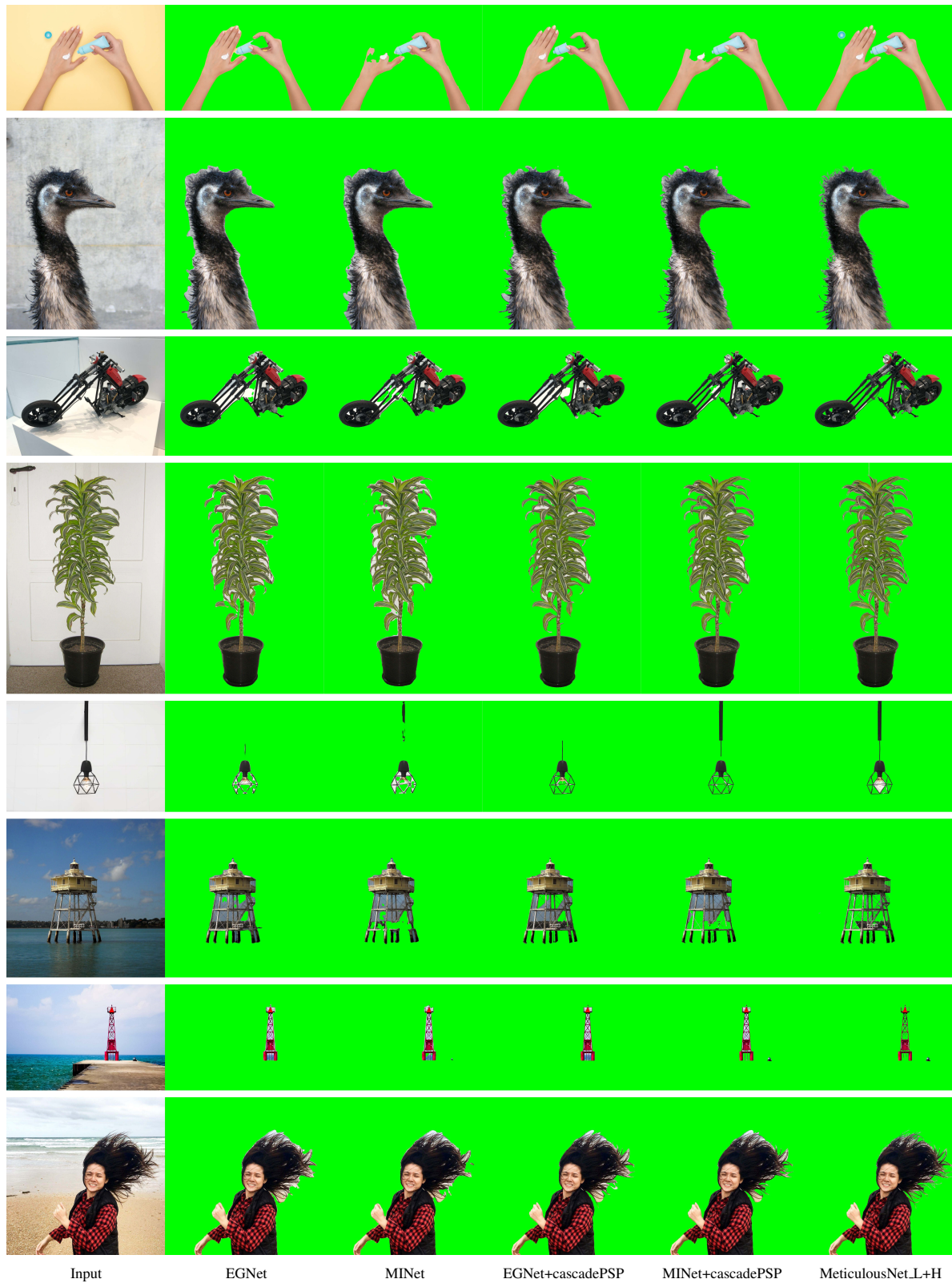
Table 6: Refinement performance on BIG dataset. All the networks refine the same prediction masks predicted by DeeplabV3+ [4]. Both the training of cascadePSP* and MeticulousNet_H include the usage of the binarized DIM data.

MQ. After adding the binarized DIM data, we observe a performance degrades for both cascadePSP* and MeticulousNet_H in IoU, which is about 0.20% decrease. This means this additional training data harm the object body segmentation. For mBA, the scenarios are different for these two networks. MeticulousNet_H can better utilize this high quality data to improve its segmentation results around object boundaries, and by contrast, cascadePSP* behave worse.

5. Ablation Studies

5.1. HierPR and Recursive Structure

We first remove all our designed structures from MeticulousNet, and name it base network, which is a PSPNet [47] with ResNet50 [7] backbone consisting of standard skip connections. Then, we add HierPR and recursive process separately into the base model. We evaluate their performances on the low resolution version of MOS600 as shown in Table 7. For HierPR, it increases both IoU, mBA and MQ by 0.17%, 1.45% and 0.69% respectively. The major improvements are on the boundary segmentation. For recursive process, it does not lead to a better IoU but improves mBA by 1.24% leading to an increase of 0.58% in MQ. When integrating these two structures together, we observe a large improvements in the object body segmentation. The IoU is increased by 2.01%, which is not expected when



Input

EGNet

MINet

EGNet+cascadePSP

MINet+cascadePSP

MeticulousNet.L+H

Figure 8: Visual comparisons among baselines and MeticulousNet (1).



Figure 9: Visual comparisons among baselines and MeticulousNet (2).

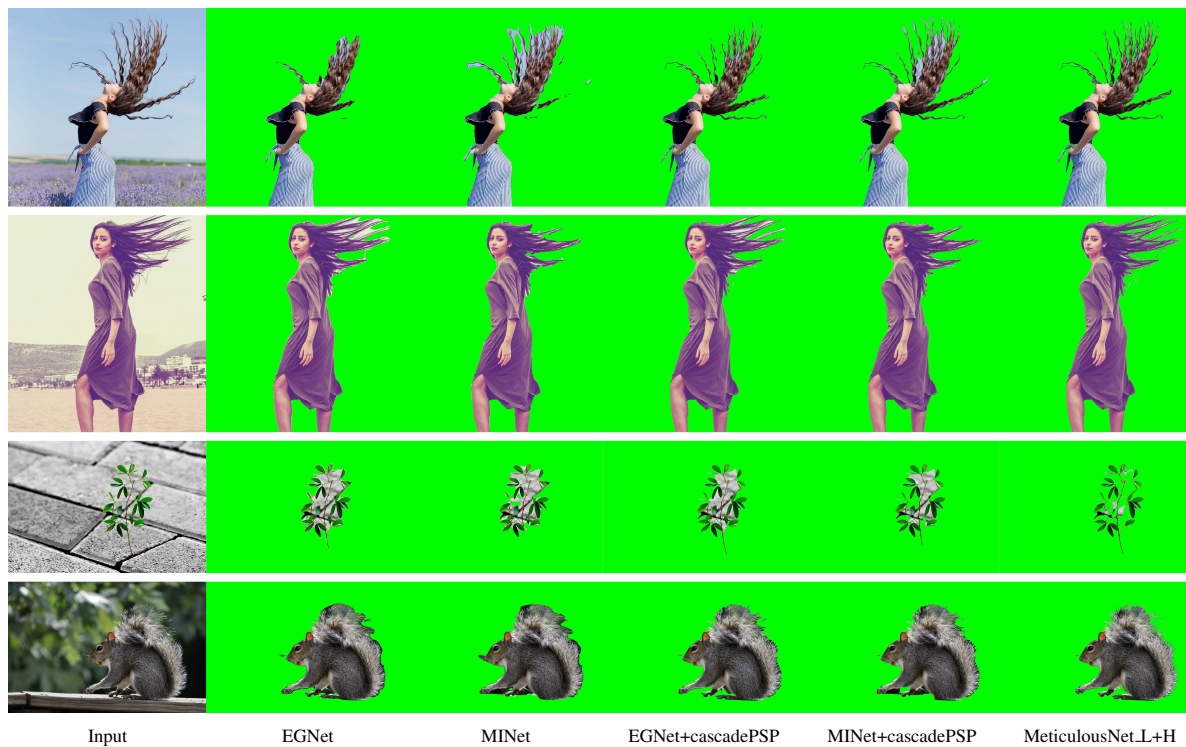


Figure 10: Visual comparisons among baselines and MeticulousNet (3).

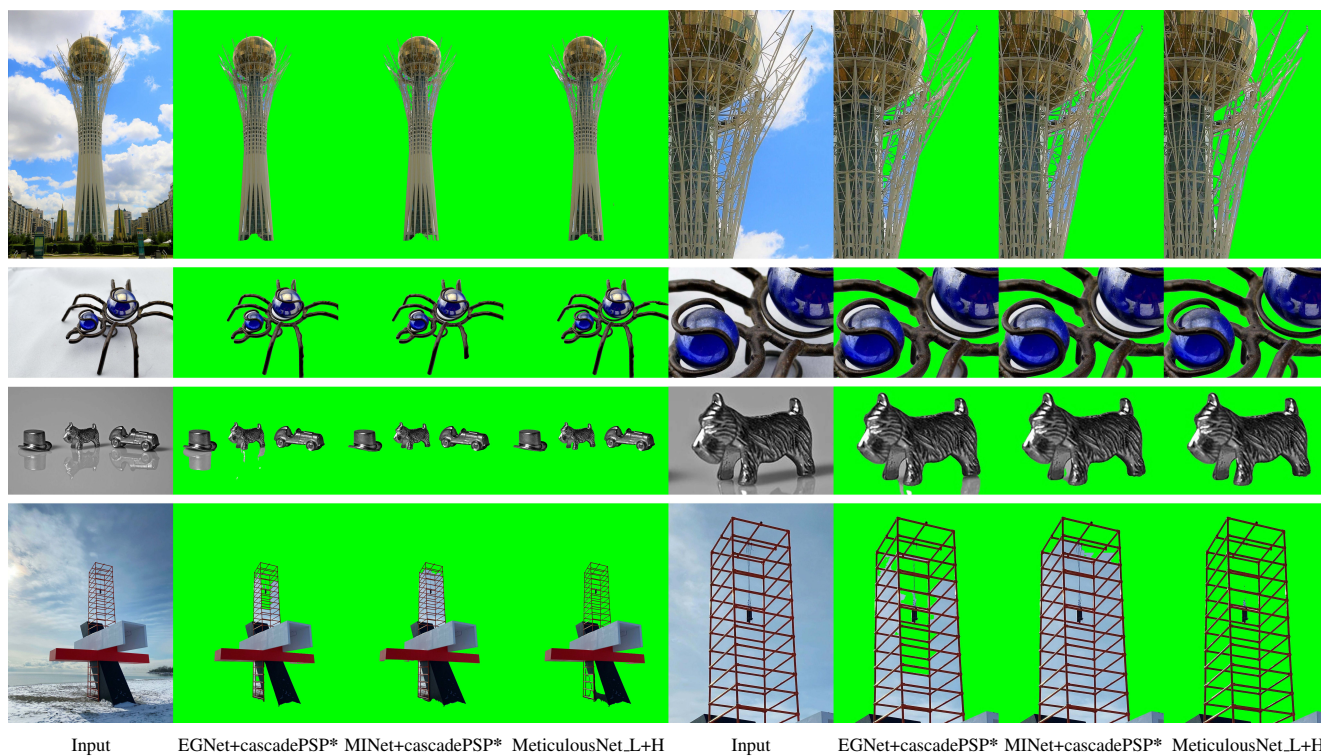


Figure 11: Visual comparisons among baselines and MeticulousNet (4). The last 4 columns are the cropped patches from the first 4 columns.

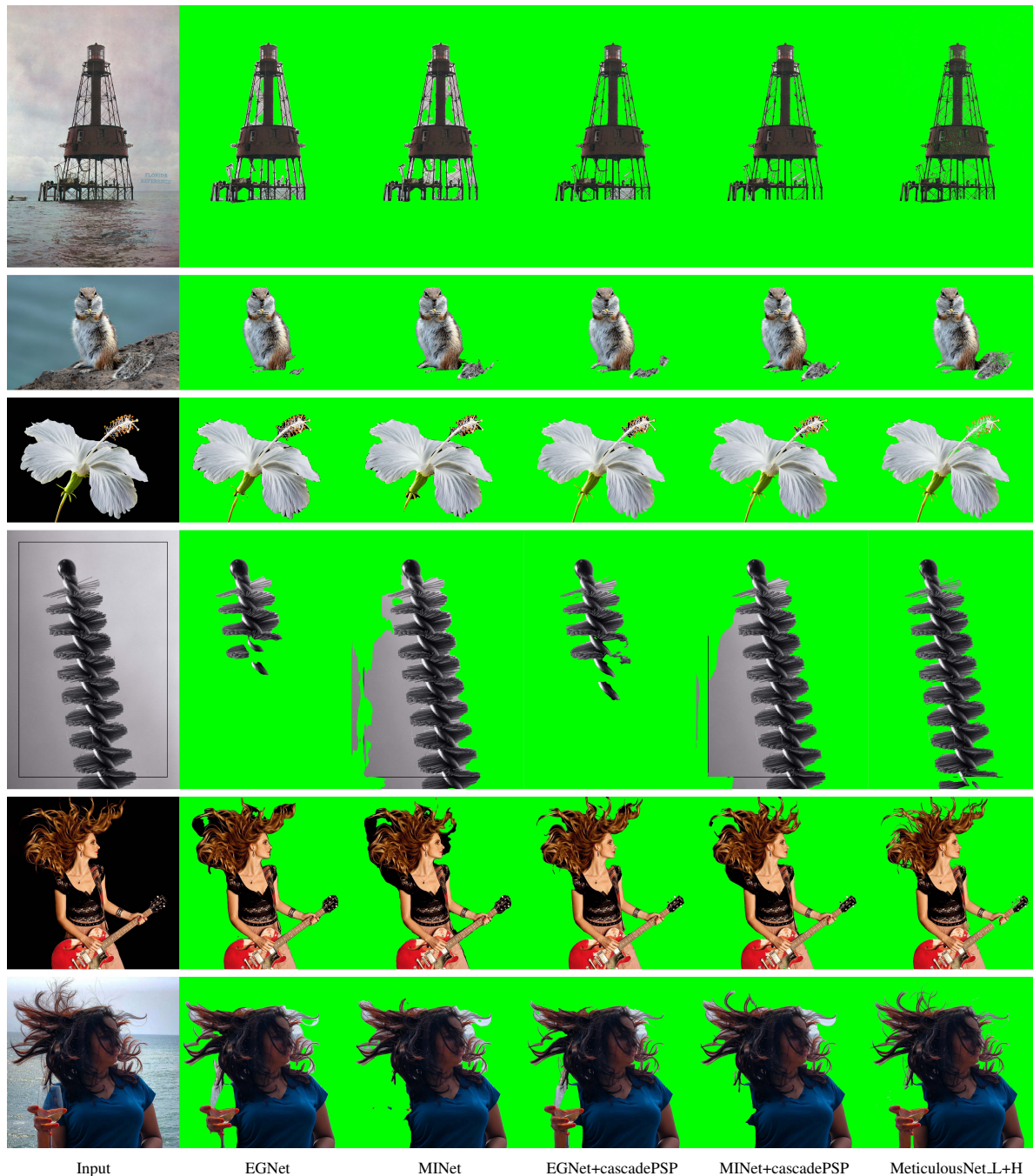


Figure 12: Failure cases.

analysing the structures separately. This indicates HierPR and recursive processes are good complementaries to be deployed together. Together, they also increase mBA and MQ by 1.93% and 1.12%, respectively. In addition, we connect our decoder with MobileNetV3 based encoder [8] leading to mobile_MeticulousNet. The number of model parameters are decreased by more than 20 times, but performance

drop in MQ is only 0.73%. This proves the flexibility and adaptability of our decoder to be used with other encoders.

5.2. Other Settings

In this part, we explore different settings for HierPR and a feasibility of the combination of a mobile encoder with the recursive decoder. In HierPR block, an area percent-

Method	IoU \uparrow	mBA \uparrow	MQ \uparrow	param. \downarrow
Base	70.17	58.79	77.04	—
Base + HierPR	70.34	60.24	77.73	—
Base + Recur	70.14	60.03	77.62	—
Base + HierPR + Recur	72.18	60.72	78.16	70.30 M
Mobile + HierPR + Recur	71.42	59.31	77.43	3.33 M

Table 7: Ablation studies on low resolution MOS600. Base and Mobile means PSPNet [47] encoder with ResNet50 [7] and MobileNetV3 [8] backbones. (Units: 1×10^{-2})

Method	IoU \uparrow	mBA \uparrow	MQ \uparrow
HierPR_20%	71.23	60.16	77.79
HierPR_15%	71.34	60.91	78.21
HierPR_10%	72.18	60.72	78.16

Table 8: Ablation studies on low resolution MOS600. We adopt HierPR_10% in our main experiments. (Units: 1×10^{-2})

age $a\%$ is specified in which it is allowed to perform refinements. In our experiments, we set this value as 10% and represent the block as HierPR_10%. We investigate whether larger area of local refinements will lead to better performances. Note that the extreme case 0% means no HierPR is applied which is discussed previously. Evaluations are shown in Table 8. We do not observe a clear benefit brought by the increase of the refinement area. Comparing HierPR_15% with HierPR_10%, although mBA is increased by 0.19% but IoU is decreased by 0.84%, making the MQ comparable in these two cases. However, when the area percentage further grows up, it will harm the performance. HierPR_20% has the worst performances.

6. Failure Case Analysis

Our method is good at capturing small details of objects, but the drawback is paying too much attention on the color variations. This causes the failure cases of two categories: First, complicated textures or other high frequency noises make the predictions unstable, as shown in the first and second examples in Figure 12. Second, local color changes break the completeness of the overall object recognition. For example, in the last row the wine glass in the hand prevent the model from recognizing the lady’s shoulder and parts of arms. We propose MeticulousNet as the first baseline for Meticulous Object Segmentation and consider overcoming the excessive attention on color variations as one of the future development directions for MOS methods.

7. Conclusion

In this work, we propose a task named Meticulous Object Segmentation (MOS). MOS is dedicated to segment

complex objects with finest details from high resolution images. This problem is essential in applied techniques such as image editing, but not well addressed in previous tasks or methods. By inviting the community to explore MOS methods, the goal of our work is to promote the emergence of novel algorithms with great applicable values.

To set up the benchmark method for MOS, we propose MeticulousNet containing a recursive decoder. The superior performances of our method compared with the combination of current state of the art models are experimentally demonstrated. We also invent Meticulous Quality and release MOS600 dataset to evaluate MOS methods.

References

- [1] Ali Borji, Ming-Ming Cheng, Qibin Hou, Huaizu Jiang, and Jia Li. Saliency object detection: A survey. *Computational visual media*, pages 1–34, 2019. [1](#), [2](#)
- [2] Ali Borji and Laurent Itti. State-of-the-art in visual attention modeling. *IEEE transactions on pattern analysis and machine intelligence*, 35(1):185–207, 2012. [2](#)
- [3] Liang-Chieh Chen, George Papandreou, Iasonas Kokkinos, Kevin Murphy, and Alan L Yuille. Semantic image segmentation with deep convolutional nets and fully connected crfs. *arXiv preprint arXiv:1412.7062*, 2014. [3](#)
- [4] Liang-Chieh Chen, Yukun Zhu, George Papandreou, Florian Schroff, and Hartwig Adam. Encoder-decoder with atrous separable convolution for semantic image segmentation. In *Proceedings of the European conference on computer vision (ECCV)*, pages 801–818, 2018. [8](#)
- [5] Ho Kei Cheng, Jihoon Chung, Yu-Wing Tai, and Chi-Keung Tang. Cascadepsp: Toward class-agnostic and very high-resolution segmentation via global and local refinement. In *Proceedings of the IEEE/CVF Conference on Computer Vision and Pattern Recognition*, pages 8890–8899, 2020. [1](#), [3](#), [4](#), [5](#), [6](#), [7](#), [8](#)
- [6] Ming-Ming Cheng, Niloy J Mitra, Xiaolei Huang, Philip HS Torr, and Shi-Min Hu. Global contrast based saliency region detection. *IEEE transactions on pattern analysis and machine intelligence*, 37(3):569–582, 2014. [2](#), [6](#)
- [7] Kaiming He, Xiangyu Zhang, Shaoqing Ren, and Jian Sun. Deep residual learning for image recognition. In *Proceedings of the IEEE conference on computer vision and pattern recognition*, pages 770–778, 2016. [2](#), [3](#), [8](#), [13](#)
- [8] Andrew Howard, Mark Sandler, Grace Chu, Liang-Chieh Chen, Bo Chen, Mingxing Tan, Weijun Wang, Yukun Zhu, Ruoming Pang, Vijay Vasudevan, et al. Searching for mobilenetv3. In *Proceedings of the IEEE International Conference on Computer Vision*, pages 1314–1324, 2019. [3](#), [12](#), [13](#)
- [9] Gao Huang, Zhuang Liu, Laurens Van Der Maaten, and Kilian Q Weinberger. Densely connected convolutional networks. In *Proceedings of the IEEE conference on computer vision and pattern recognition*, pages 4700–4708, 2017. [2](#)
- [10] Laurent Itti, Christof Koch, and Ernst Niebur. A model of saliency-based visual attention for rapid scene analysis.

- IEEE Transactions on pattern analysis and machine intelligence*, 20(11):1254–1259, 1998. 2
- [11] Alexander Kirillov, Yuxin Wu, Kaiming He, and Ross Girshick. Pointrend: Image segmentation as rendering. In *Proceedings of the IEEE/CVF Conference on Computer Vision and Pattern Recognition*, pages 9799–9808, 2020. 3
- [12] Dominik A Klein and Simone Frintrap. Center-surround divergence of feature statistics for salient object detection. In *2011 International Conference on Computer Vision*, pages 2214–2219. IEEE, 2011. 2
- [13] Philipp Krähenbühl and Vladlen Koltun. Efficient inference in fully connected crfs with gaussian edge potentials. In *Advances in neural information processing systems*, pages 109–117, 2011. 3
- [14] Alex Krizhevsky, Ilya Sutskever, and Geoffrey E Hinton. Imagenet classification with deep convolutional neural networks. In *Advances in neural information processing systems*, pages 1097–1105, 2012. 2
- [15] Guanbin Li and Yizhou Yu. Visual saliency based on multi-scale deep features. In *Proceedings of the IEEE conference on computer vision and pattern recognition*, pages 5455–5463, 2015. 2
- [16] Xiang Li, Tianhan Wei, Yau Pun Chen, Yu-Wing Tai, and Chi-Keung Tang. Fss-1000: A 1000-class dataset for few-shot segmentation. In *Proceedings of the IEEE/CVF Conference on Computer Vision and Pattern Recognition*, pages 2869–2878, 2020. 6
- [17] Guosheng Lin, Anton Milan, Chunhua Shen, and Ian Reid. Refinenet: Multi-path refinement networks for high-resolution semantic segmentation. In *Proceedings of the IEEE conference on computer vision and pattern recognition*, pages 1925–1934, 2017. 3
- [18] Guosheng Lin, Chunhua Shen, Anton Van Den Hengel, and Ian Reid. Efficient piecewise training of deep structured models for semantic segmentation. In *Proceedings of the IEEE conference on computer vision and pattern recognition*, pages 3194–3203, 2016. 3
- [19] Tsung-Yi Lin, Michael Maire, Serge Belongie, James Hays, Pietro Perona, Deva Ramanan, Piotr Dollár, and C Lawrence Zitnick. Microsoft coco: Common objects in context. In *European conference on computer vision*, pages 740–755. Springer, 2014. 6
- [20] Nian Liu and Junwei Han. Dhsnet: Deep hierarchical saliency network for salient object detection. In *Proceedings of the IEEE Conference on Computer Vision and Pattern Recognition*, pages 678–686, 2016. 2
- [21] Nian Liu, Junwei Han, and Ming-Hsuan Yang. Picanet: Learning pixel-wise contextual attention for saliency detection. In *Proceedings of the IEEE Conference on Computer Vision and Pattern Recognition*, pages 3089–3098, 2018. 2
- [22] Jonathan Long, Evan Shelhamer, and Trevor Darrell. Fully convolutional networks for semantic segmentation. In *Proceedings of the IEEE conference on computer vision and pattern recognition*, pages 3431–3440, 2015. 2
- [23] Zhiming Luo, Akshaya Mishra, Andrew Achkar, Justin Eichel, Shaozi Li, and Pierre-Marc Jodoin. Non-local deep features for salient object detection. In *Proceedings of the IEEE Conference on computer vision and pattern recognition*, pages 6609–6617, 2017. 2
- [24] Robert Osserman et al. The isoperimetric inequality. *Bulletin of the American Mathematical Society*, 84(6):1182–1238, 1978. 6
- [25] Youwei Pang, Xiaoqi Zhao, Lihe Zhang, and Huchuan Lu. Multi-scale interactive network for salient object detection. In *Proceedings of the IEEE/CVF Conference on Computer Vision and Pattern Recognition*, pages 9413–9422, 2020. 1, 2, 3, 6, 7
- [26] Chao Peng, Xiangyu Zhang, Gang Yu, Guiming Luo, and Jian Sun. Large kernel matters—improve semantic segmentation by global convolutional network. In *Proceedings of the IEEE conference on computer vision and pattern recognition*, pages 4353–4361, 2017. 3
- [27] Olaf Ronneberger, Philipp Fischer, and Thomas Brox. U-net: Convolutional networks for biomedical image segmentation. In *International Conference on Medical image computing and computer-assisted intervention*, pages 234–241. Springer, 2015. 2
- [28] Xiaoyong Shen, Aaron Hertzmann, Jiaya Jia, Sylvain Paris, Brian Price, Eli Shechtman, and Ian Sachs. Automatic portrait segmentation for image stylization. In *Computer Graphics Forum*, volume 35, pages 93–102. Wiley Online Library, 2016. 1
- [29] Jianping Shi, Qiong Yan, Li Xu, and Jiaya Jia. Hierarchical image saliency detection on extended cssd. *IEEE transactions on pattern analysis and machine intelligence*, 38(4):717–729, 2015. 6
- [30] Karen Simonyan and Andrew Zisserman. Very deep convolutional networks for large-scale image recognition. *arXiv preprint arXiv:1409.1556*, 2014. 2
- [31] Christian Szegedy, Wei Liu, Yangqing Jia, Pierre Sermanet, Scott Reed, Dragomir Anguelov, Dumitru Erhan, Vincent Vanhoucke, and Andrew Rabinovich. Going deeper with convolutions. In *Proceedings of the IEEE conference on computer vision and pattern recognition*, pages 1–9, 2015. 2
- [32] Jingdong Wang, Ke Sun, Tianheng Cheng, Borui Jiang, Chaorui Deng, Yang Zhao, Dong Liu, Yadong Mu, Mingkui Tan, Xinggang Wang, et al. Deep high-resolution representation learning for visual recognition. *IEEE transactions on pattern analysis and machine intelligence*, 2020. 1
- [33] Lijun Wang, Huchuan Lu, Xiang Ruan, and Ming-Hsuan Yang. Deep networks for saliency detection via local estimation and global search. In *Proceedings of the IEEE Conference on Computer Vision and Pattern Recognition*, pages 3183–3192, 2015. 2
- [34] Lijun Wang, Huchuan Lu, Yifan Wang, Mengyang Feng, Dong Wang, Baocai Yin, and Xiang Ruan. Learning to detect salient objects with image-level supervision. In *Proceedings of the IEEE Conference on Computer Vision and Pattern Recognition*, pages 136–145, 2017. 6
- [35] Linzhao Wang, Lijun Wang, Huchuan Lu, Pingping Zhang, and Xiang Ruan. Saliency detection with recurrent fully convolutional networks. In *European conference on computer vision*, pages 825–841. Springer, 2016. 2

- [36] Yichen Wei, Fang Wen, Wangjiang Zhu, and Jian Sun. Geodesic saliency using background priors. In *European conference on computer vision*, pages 29–42. Springer, 2012. [2](#)
- [37] Ning Xu, Brian Price, Scott Cohen, and Thomas Huang. Deep image matting. In *Proceedings of the IEEE Conference on Computer Vision and Pattern Recognition*, pages 2970–2979, 2017. [6](#)
- [38] Chuan Yang, Lihe Zhang, Huchuan Lu, Xiang Ruan, and Ming-Hsuan Yang. Saliency detection via graph-based manifold ranking. In *Proceedings of the IEEE conference on computer vision and pattern recognition*, pages 3166–3173, 2013. [2](#), [6](#)
- [39] Yi Zeng, Pingping Zhang, Jianming Zhang, Zhe Lin, and Huchuan Lu. Towards high-resolution salient object detection. In *Proceedings of the IEEE International Conference on Computer Vision*, pages 7234–7243, 2019. [2](#), [3](#), [5](#), [6](#)
- [40] Chi Zhang, Guosheng Lin, Fayao Liu, Rui Yao, and Chunhua Shen. Canet: Class-agnostic segmentation networks with iterative refinement and attentive few-shot learning. In *Proceedings of the IEEE Conference on Computer Vision and Pattern Recognition*, pages 5217–5226, 2019. [3](#)
- [41] Jianming Zhang and Stan Sclaroff. Saliency detection: A boolean map approach. In *Proceedings of the IEEE international conference on computer vision*, pages 153–160, 2013. [2](#)
- [42] Lihe Zhang, Jianwu Ai, Bowen Jiang, Huchuan Lu, and Xiukui Li. Saliency detection via absorbing markov chain with learnt transition probability. *IEEE Transactions on Image Processing*, 27(2):987–998, 2017. [2](#)
- [43] Lu Zhang, Ju Dai, Huchuan Lu, You He, and Gang Wang. A bi-directional message passing model for salient object detection. In *Proceedings of the IEEE Conference on Computer Vision and Pattern Recognition*, pages 1741–1750, 2018. [2](#)
- [44] Lihe Zhang, Chuan Yang, Huchuan Lu, Xiang Ruan, and Ming-Hsuan Yang. Ranking saliency. *IEEE transactions on pattern analysis and machine intelligence*, 39(9):1892–1904, 2016. [2](#)
- [45] Pingping Zhang, Dong Wang, Huchuan Lu, Hongyu Wang, and Xiang Ruan. Amulet: Aggregating multi-level convolutional features for salient object detection. In *Proceedings of the IEEE International Conference on Computer Vision*, pages 202–211, 2017. [2](#)
- [46] Xiaoning Zhang, Tiantian Wang, Jinqing Qi, Huchuan Lu, and Gang Wang. Progressive attention guided recurrent network for salient object detection. In *Proceedings of the IEEE Conference on Computer Vision and Pattern Recognition*, pages 714–722, 2018. [2](#)
- [47] Hengshuang Zhao, Jianping Shi, Xiaojuan Qi, Xiaogang Wang, and Jiaya Jia. Pyramid scene parsing network. In *Proceedings of the IEEE conference on computer vision and pattern recognition*, pages 2881–2890, 2017. [3](#), [8](#), [13](#)
- [48] Jia-Xing Zhao, Jiang-Jiang Liu, Deng-Ping Fan, Yang Cao, Jufeng Yang, and Ming-Ming Cheng. Egnet: Edge guidance network for salient object detection. In *Proceedings of the IEEE International Conference on Computer Vision*, pages 8779–8788, 2019. [1](#), [2](#), [3](#), [7](#)
- [49] Rui Zhao, Wanli Ouyang, Hongsheng Li, and Xiaogang Wang. Saliency detection by multi-context deep learning. In *Proceedings of the IEEE conference on computer vision and pattern recognition*, pages 1265–1274, 2015. [2](#)
- [50] Shuai Zheng, Sadeep Jayasumana, Bernardino Romera-Paredes, Vibhav Vineet, Zhizhong Su, Dalong Du, Chang Huang, and Philip HS Torr. Conditional random fields as recurrent neural networks. In *Proceedings of the IEEE international conference on computer vision*, pages 1529–1537, 2015. [3](#)
- [51] Wangjiang Zhu, Shuang Liang, Yichen Wei, and Jian Sun. Saliency optimization from robust background detection. In *Proceedings of the IEEE conference on computer vision and pattern recognition*, pages 2814–2821, 2014. [2](#)